Expanded View Figures

Figure EV1. Incorporation of H3.3 at pat-PCH in mouse zygotes requires interaction between histone H3.3 and H3.3-specific chaperones.

A Experimental design for live imaging of exogenously provided H3.3, H3.2, H3.3^{G90M}, H3.3$^{A87S/I89V/G90M}$, and DAXX proteins in wild-type, *Daxx* conditionally deficient or siRNA-treated mouse zygotes. mRNA transcripts and siRNAs were microinjected in MII-arrested oocytes, which were subsequently fertilized by injection of sperm (ICSI).

B Still images of time-lapse imaging of first cell cycle showing temporal and spatial dynamics of H3.3-mCherry and H3.3$^{A87S/I89V/G90M}$-EGFP proteins in wild-type zygotes (n = 8). The data demonstrate that interactions with H3.3-specific chaperone(s) are required for H3.3 deposition into the paternal genome shortly after fertilization (PN0) and into pat-PCH during/after replication (PN5; yellow arrowhead). Except for PCH, exogenous H3.3$^{A87S/I89V/G90M}$ is incorporated during S phase throughout paternal and maternal genomes, presumably in a replication-mediated manner. Yellow dashed circles represent the contours of the pronuclei. Scale bar, 15 μm.

C Still images of time-lapse imaging of first cell cycle showing temporal and spatial dynamics of H3.3-mCherry and H3.3^{G90M}-EGFP proteins in wild-type zygotes (n = 8). As in the H3.3$^{A87S/I89V/G90M}$ triple substitution mutant, the G90M substitution is sufficient to inhibit H3.3-chaperone-dependent H3.3 deposition in the decondensing sperm genome and into pat-PCH during/after replication (PN5; yellow arrowhead). Yellow dashed circles represent the contours of the pronuclei. Scale bar, 15 μm.

D Heatmaps showing mRNA expression levels of histone H3 chaperones and various chromatin associated proteins during early embryogenesis (Park *et al*, 2013).

E IF detection of ATRX in wild-type (WT) (n = 22), *HP1β*-deficient (n = 8), and *Suv39h2*-deficient (n = 18) germinal vesicle (GV) stage oocytes. Arrowheads point to location of PCH in oocyte nuclei. Scale bar, 10 μm.

F IF detection of DAXX in wild-type (WT) (n = 26), *HP1β*-deficient (n = 11), and *Suv39h2*-deficient (n = 7) GV oocytes. Arrowheads point to location of PCH in oocyte nuclei. Scale bar, 10 μm.

G Still images of time-lapse imaging of first cell cycle showing temporal and spatial dynamics of DAXX-EGFP in wild-type zygotes (n = 19). DAXX-EGFP localizes at pat-PCH throughout the first cell cycle. Zoom-up image shows magnification of DAXX-EGFP localization at pat-PCH in decondensing sperm (yellow box in PN0 image). Scale bar, 10 μm.

H Top: IF detection of DAXX and ATRX at pat-PCH in WT PN5 zygotes. Bottom: Fluorescence intensity profiles of DAXX and ATRX along white crescent line in the top panel at pat-PCH of zygotes. Scale bars, 5 μm.

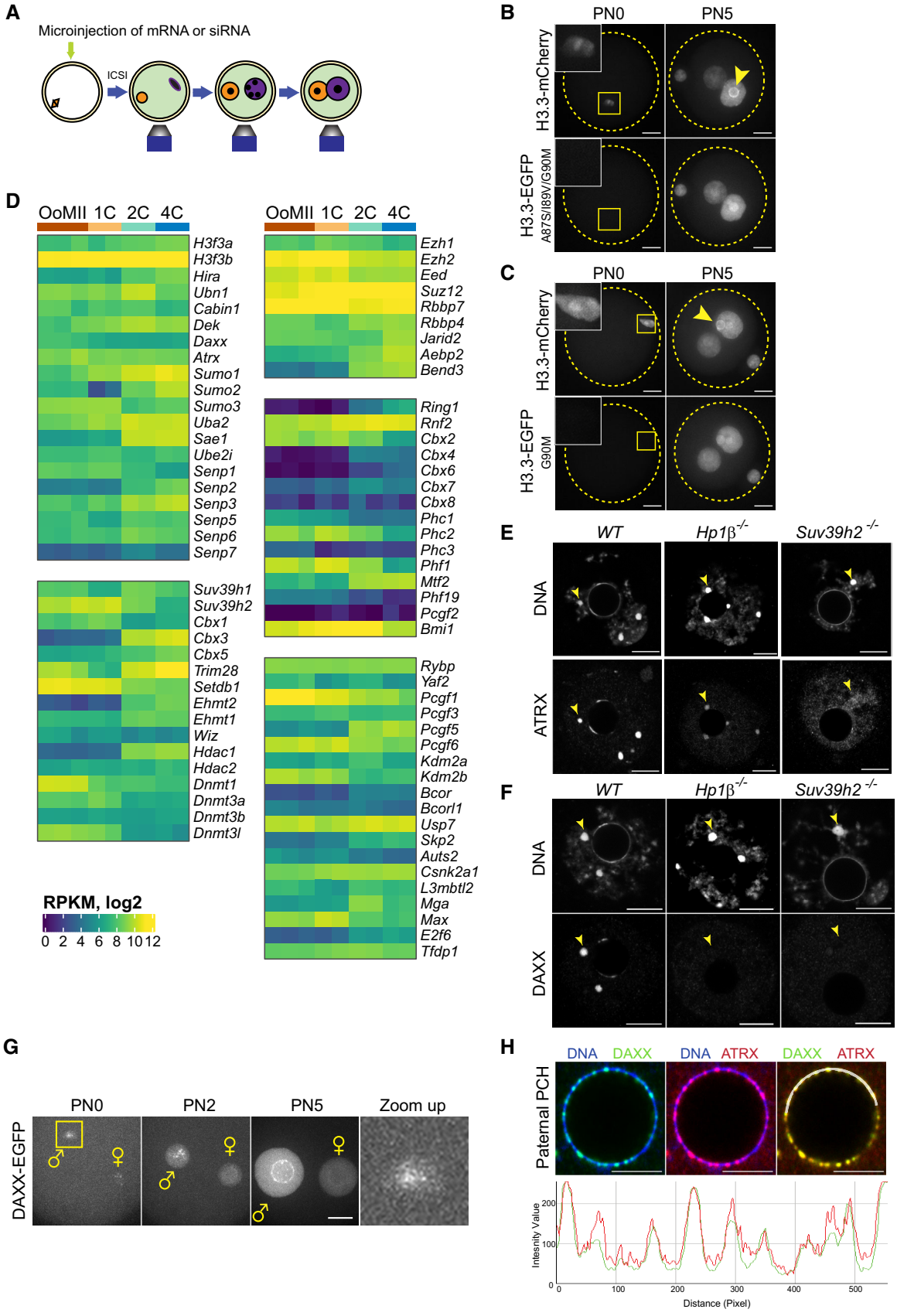

Figure EV1.

Figure EV2. CBX2-dependent targeting of DAXX to PRC1 target genes.

A Left: Schematic diagrams of hCBX2.1, hCBX2.2, and mCBX7 proteins illustrating location of functional domains. Right: legend for panels (B and D).

B ChIP-qPCR analyses of chromatin isolated from HEK293^{5xUAS} cells expressing either the full-length ^{GAL4DBD}CBX2.1, the short isoform ^{GAL4DBD}CBX2.2, or ^{GAL4DBD}CBX7 in combination with DAXX^{MycHis} show that DAXX is efficiently recruited by CBX2.1 to the 5xUAS site, while CBX2.2 and CBX7 are inefficient. Data are means ± SEM (n = 3).

C Co-immunoprecipitation of DAXX^{MycHis} with CBX2-EGFP, CBX7-EGFP, or RYBP-EGFP proteins expressed in HEK293T cells. DAXX^{MycHis} was more efficiently recovered with CBX2-EGFP.

D ChIP-qPCR analyses of chromatin isolated from HEK293^{5xUAS} cells expressing either the full-length ^{GAL4DBD}CBX2.1, the short isoform ^{GAL4DBD}CBX2.2, or ^{GAL4DBD}CBX7 in combination with DAXX^{MycHis} show that DAXX is efficiently recruited by CBX2.1 to the promoter of *RUNX1*, while CBX2.2 and CBX7 are inefficient. Data are means ± SEM (n = 3).

E Browser plot showing occupancy for ^{Gal4DBD}CBX2.1 and DAXX^{MycHis} proteins along the *HOXA* cluster genes in the genome of HEK293^{5xUAS} cells expressing the proteins indicated on the right.

F ChIP-seq analysis of ^{GAL4DBD}CBX2.2 occupancy in HEK293^{5xUAS} cells expressing DAXX^{MycHis} (x-axis) versus ^{GAL4DBD}CBX2.2 and DAXX^{MycHis} (y-axis) showing ($\log_2$) enrichment for ^{GAL4DBD}CBX2.2 only at a few TSSs (± 1 kb) in cells expressing the CBX2.2 protein (y-axis).

G ChIP-seq analysis of ^{GAL4DBD}CBX2.2 versus DAXX^{MycHis} occupancy in HEK293^{5xUAS} cells expressing ^{GAL4DBD}CBX2.2 and DAXX^{MycHis}, revealing poor correlation between enrichment levels ($\log_2$) of both proteins at TSSs. TSSs highlighted in red show enrichment with anti-Myc antibody independently of ^{GAL4DBD}CBX2.2 occupancy.

H ChIP-seq analysis of DAXX^{MycHis} occupancy in HEK293^{5xUAS} cells expressing DAXX^{MycHis} (x-axis) versus ^{GAL4DBD}CBX2.2 and DAXX^{MycHis} (y-axis) showing largely comparable enrichment ($\log_2$) for DAXX^{MycHis} at TSS of few genes, irrespective whether CBX2.2 is expressed (y-axis), indicating that CBX2.2 does not target DAXX to chromatin. TSSs highlighted in red show enrichment with anti-Myc antibody independently of ^{GAL4DBD}CBX2.2 occupancy.

Source data are available online for this figure.

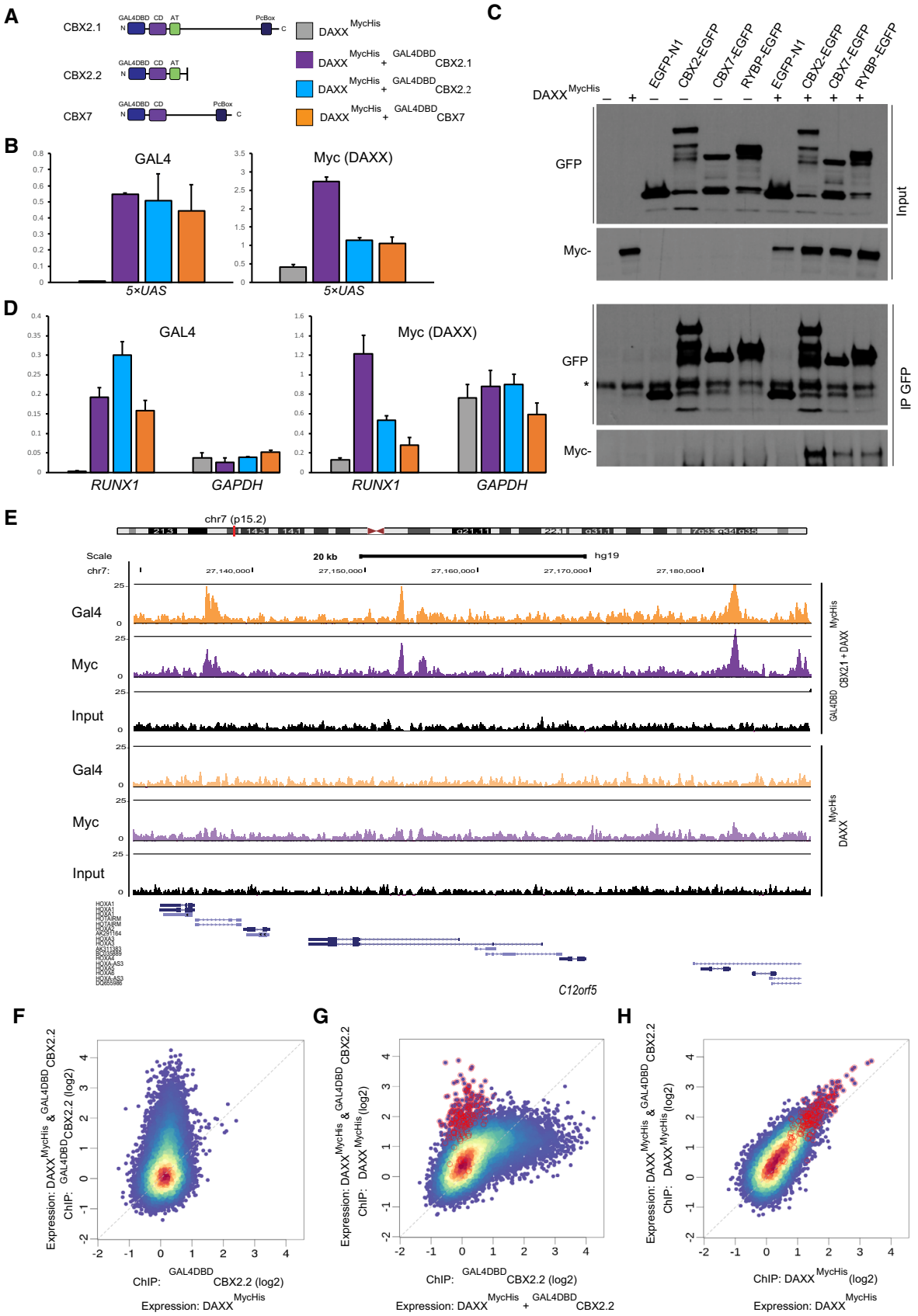

Figure EV2.

Figure EV3. SUMO-dependent targeting of DAXX to subnuclear regions and PRC1 target genes, and characterization of *Daxx* maternally deficient zygotes.

A IF co-localization of DAXX and SUMO1 or SUMO2/3 at PML bodies in wild-type mouse embryonic stem cells (mESCs).

B Top: IF co-localization of SUMO2/3 and ATRX on pat-PCH in WT PN5 zygotes (n = 14). Bottom: Fluorescence intensity profiles of SUMO2/3 and ATRX along white line in top panel at pat-PCH of zygotes. Scale bar, 5 μm.

C IF detection of SUMO2/3 and wild-type and mutant Myc-tagged DAXX proteins in mESCs. Mutations in both SUMO-interacting motifs (SIM) abrogate co-localization of DAXX with SUMO2/3-labeled PML bodies.

D Western blot showing similar expression levels of tagged proteins in HEK293^{5xUAS} cells used for ChIP-qPCR experiments shown in Figs 4B and EV3E.

E ChIP-qPCR analyses of chromatin isolated from HEK293^{5xUAS} cells expressing either the full-length DAXX^{MycHis} or DAXX^{MycHis} without SIM domains in combination with ^{GAL4DBD}CBX2.1 show that DAXX is efficiently recruited by CBX2.1 to the promoter of *CCND2* and *RUNX1*, while DAXX$^{\Delta SIM1/2}$ is inefficient. Data are means ± SEM (n = 3).

F Schematic diagram of *Daxx* wild-type, floxed, and mutant alleles. *Zp3-cre*-mediated excision of exon 3 will induce a progressive depletion of DAXX protein in growing oocytes.

G IF detection of DAXX in paternal pronuclei of wild-type (n = 16) and *Daxx*$^{m-z+}$ zygotes (n = 19). Yellow dashed circles represent the contours of the pronuclei.

H IF detection of H2AK119 monoubiquitination (H2AK119ub1) in paternal pronuclei of wild-type (n = 28) and *Daxx*$^{m-z+}$ (n = 21) zygotes, demonstrating no change in PRC1-catalyzed H2AK119ub1 at PCH (Tardat *et al*, 2015). Yellow dashed circles represent the contours of the pronuclei.

I Ni-pulldown of ^{6xHis}SUMO2-conjugated proteins from HEK293 extracts transiently expressing either wild-type, CBX2 with Polycomb box mutation (Pc-Box) or CBX2.1 with K154R and K350R substitutions. CBX2 and SUMO2-conjugated CBX2 were detected with an anti-GFP antibody.

J IF detection of EGFP-tagged proteins shows that CBX2^{4KR}-EGFP binds to condensed paternal metaphase chromosomes during the first cleavage division in zygotes as CBX2-EGFP does. The dashed line separates the chromosomes of paternal and maternal origins.

Data information: Scale bar, 10 μm.
Source data are available online for this figure.

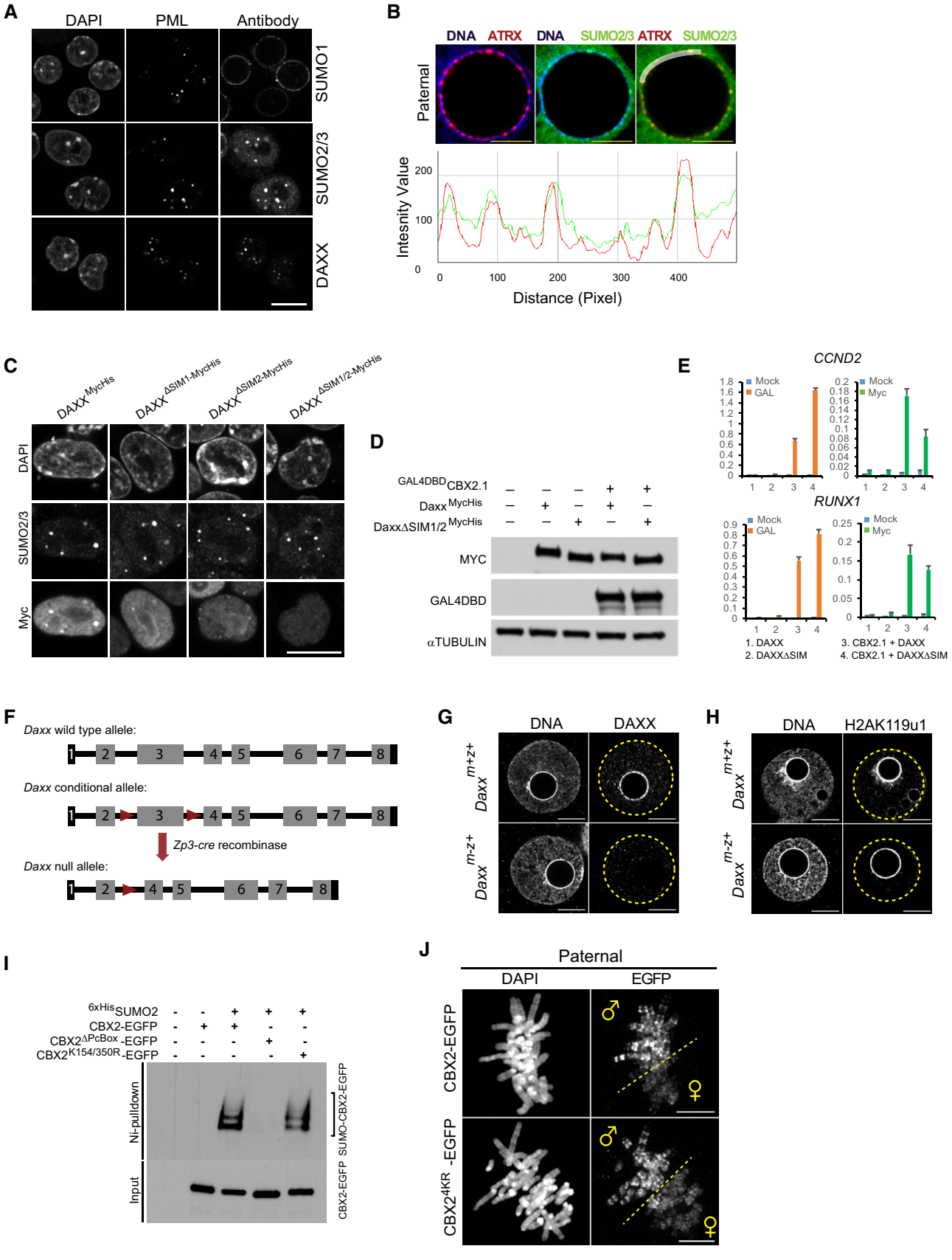

Figure EV3.

Figure EV4. Maternally *Daxx* deficient embryos display genome instability.

A IF detection of micronuclei and γH2A in *Daxx*$^{m+z+}$, *Daxx*$^{m-z+}$, *and Daxx*$^{m-z-}$ embryos at the 4/8-cell stage. A chromosome broken within the PCH region was stained by γH2A (yellow box). Arrowheads point to micronuclei.

B IF detection of DAXX and ATRX in wild-type (n = 46) and *Daxx*$^{m-z+}$ (n = 41) 2-cell embryos showing differential localization of both proteins at pat- and mat-PCH. A micronucleus in a *Daxx*$^{m-z+}$ 2-cell embryo lacks ATRX staining, illustrating its paternal origin (yellow arrowhead). The dashed line separates approximately the chromatin of paternal and maternal origins.

C IF detection of 5mC and 5hmC in *Daxx*$^{m+z+}$ (n = 6) and *Daxx*$^{m-z+}$ (n = 9) late zygotes.

D DNA FISH for major and minor satellites on cleavage chromosomes of *Daxx*$^{m-z+}$ and *Ring1*$^{m-z+}$; *Rnf2*$^{m-z+}$ zygotes showing aberrant stretching of major satellite sequences (yellow arrowheads).

E Live imaging of *Daxx*$^{m-z+}$ zygotes labeled with H2B-mCherry showing stretching of proximal end of an acrocentric chromosome (white arrow heads) despite localization of exogenous DAXX^{R244A}-EGFP at pat-PCH (white star).

F IF of DAXX protein in *Daxx*$^{m+z+}$ (n = 19) and *Daxx*$^{m-z+}$ (n = 45) 4-cell embryos displaying normal chromocenter formation in the absence of DAXX protein. Arrowhead points to large micronucleus.

G IF staining of DAXX and PML proteins showing focal co-localization in wt 8-cell embryos (n = 15) (arrowheads). DAXX localizes to DAPI-bright PCH as well.

Data information: Scale bars, 10 μm.

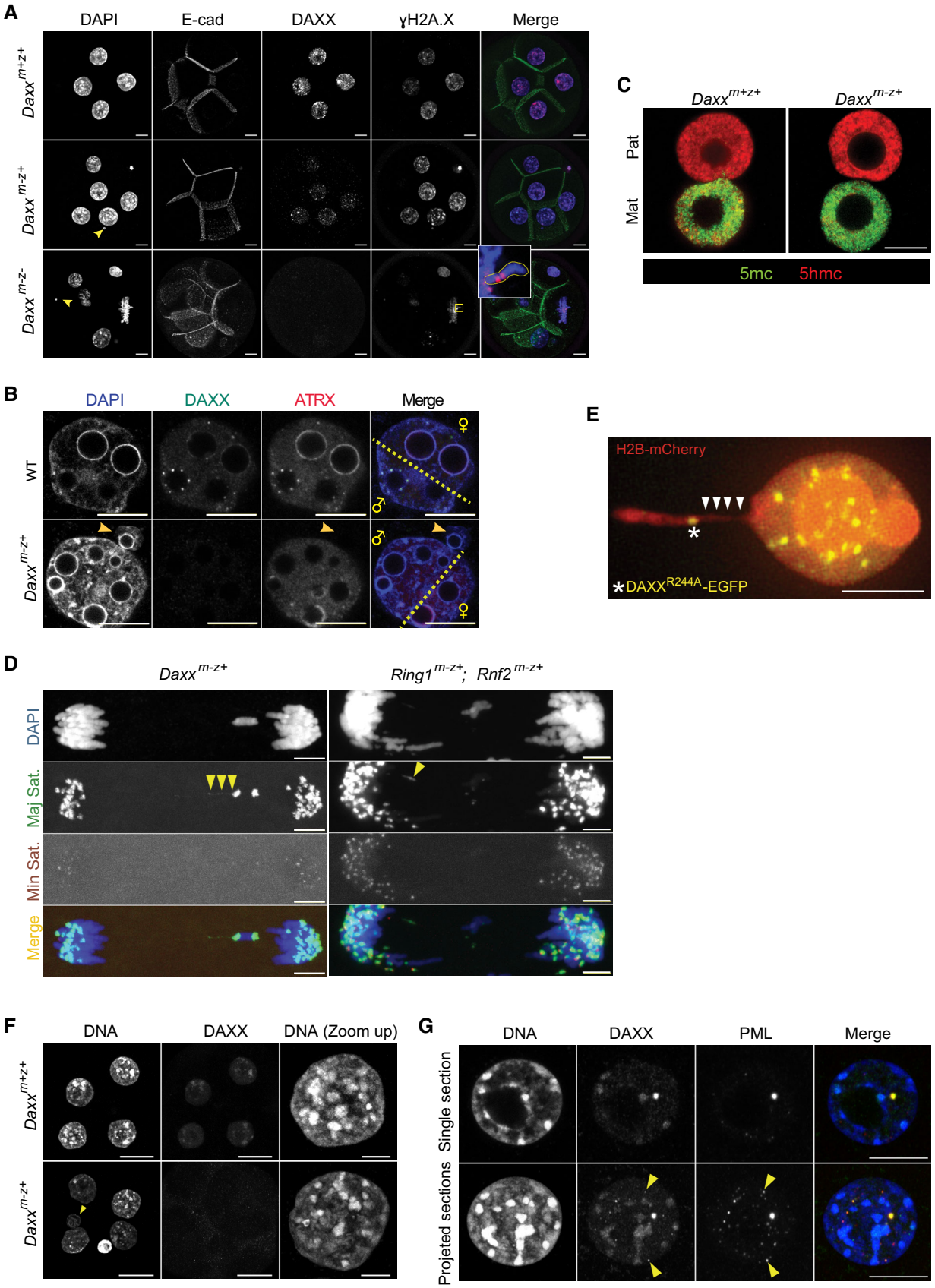

Figure EV4.

Figure EV5. DAXX contributes to *PRC1*- but not to *Setdb1*-mediated gene repression in mouse oocytes.

A RNA sequencing information of data presented in this study.

B Overview of RNA-Seq datasets at the *Daxx* genomic locus. A genomic snapshot shows abundance of RNA-Seq read ends summarized for genomic bins of 10 bp and normalized by total number of mapped reads in each library. Splice junctions are visualized using sashimi plots below each track where the widths of the lines correspond to normalized read counts supporting each splice junction and numbers below each line represent raw (not normalized) read counts supporting each splice junction in each sample. Splice junctions supported by less than 5 reads are not shown. Biological replicates were merged. The cartoon below the tracks illustrates the longest transcript of *Daxx*. The triangles below indicate the position of the loxP sites flanking exon 3 of the corresponding floxed *Daxx* gene allele.

C Scatter plot showing fold change (FC) (in $\log_2$) in gene expression between indicated samples. Dotted lines indicated $\log_2$ (FC) of 1.

D Venn diagrams showing overlap in genes up- or downregulated in *Daxx*-deficient versus control MII oocytes in comparison with genes up- or downregulated in *Ring1*; *Rnf2* double deficient versus control GV oocytes. Comparisons are given for two different statistical criteria.

E Boxplots showing FC ($\log_2$) in gene expression between *Setdb1*-deficient versus control GV oocytes for three groups of genes classified according to H3K27me3 enrichments in WT MII oocytes (as shown in Fig 7E). Lower hinge, central line, and upper hinge represent 25^{th}, 50^{th} (median), and 75^{th} percentiles, respectively. Upper/lower whiskers extend to the largest/smallest values no further than 1.5*IQR from the upper/lower hinge, where IQR is interquartile range or distance between 25^{th} and 75^{th} percentiles. Outliers are not displayed. The notches extend $1.5*IQR/\sqrt{n}$ where n is a number of genes in each H3K27me3 class. A number of genes (n) in "Low", "Medium", and "High" H3K27me3 class used for boxplots are 9824, 2311, and 2647, respectively. Expression changes were estimated using three biological replicates for each condition. Statistical significance was estimated using two-sided *t*-tests.

F Boxplot showing FC ($\log_2$) in gene expression between *Setdb1*-deficient and control GV oocytes for five groups of genes classified according to FC ($\log_2$) in gene expression between *Ring1 Rnf2*-deficient and control GV oocytes. Boxplots are created similarly to (E), and the number of genes used for each boxplot is displayed below. Expression changes were estimated using three biological replicates. Statistical significance was estimated using two-sided *t*-tests.

G Schematic diagram of the mouse CBX2 protein illustrating the sequence domains and their associated chromatin functions. For further explanations, see end of discussion of manuscript.

A

Sample	#Total reads	#Mapped reads	%Mapped
Daxx_MII_oocyte_F/F_1	59,430,750	49,889,964	83.95%
Daxx_MII_oocyte_F/F_2	73,457,225	61,420,841	83.61%
Daxx_MII_oocyte_F/F_3	68,782,691	57,661,638	83.83%
Daxx_MII_oocyte_F/F_Zp3-cre_1	68,012,176	57,836,540	85.04%
Daxx_MII_oocyte_F/F_Zp3-cre_2	70,396,715	58,123,809	82.57%
Daxx_MII_oocyte_F/F_Zp3-cre_3	69,212,495	58,206,775	84.10%
Daxx_2cell_F/+_1	64,943,086	43,674,344	67.25%
Daxx_2cell_F/+_2	109,244,803	61,148,599	55.97%
Daxx_2cell_F/+_3	101,940,736	64,725,283	63.49%
Daxx_2cell_-/+_Zp3-cre_2	115,844,738	72,362,874	62.47%
Daxx_2cell_-/+_Zp3-cre_3	90,570,112	56,759,094	62.67%
PRC1_GV_oocyte_Ring1_KO_Rnf2_F/F_1	38,686,114	34,894,477	90.20%
PRC1_GV_oocyte_Ring1_KO_Rnf2_F/F_2	34,158,351	30,972,238	90.67%
PRC1_GV_oocyte_Ring1_KO_Rnf2_F/F_3	39,134,914	35,202,215	89.95%
PRC1_GV_oocyte_Ring1_KO_Rnf2_F/F1_Zp3-cre_1	30,313,358	24,962,724	82.35%
PRC1_GV_oocyte_Ring1_KO_Rnf2_F/F1_Zp3-cre_2	30,377,560	27,217,609	89.60%
PRC1_GV_oocyte_Ring1_KO_Rnf2_F/F1_Zp3-cre_3	41,174,472	37,025,544	89.92%

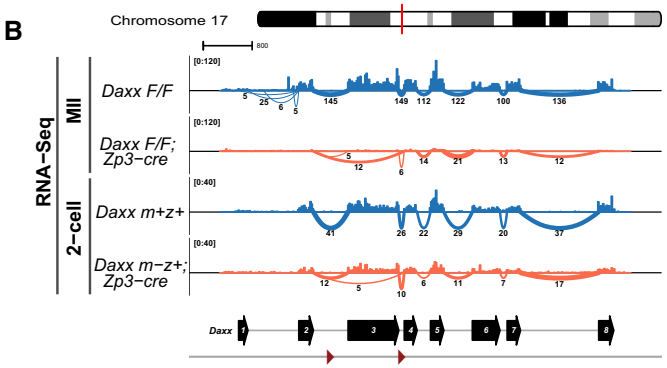

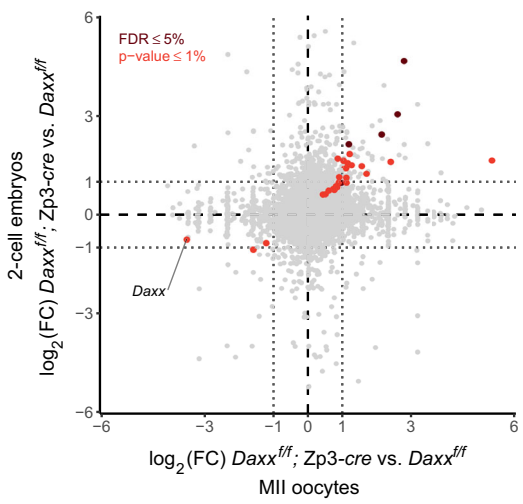

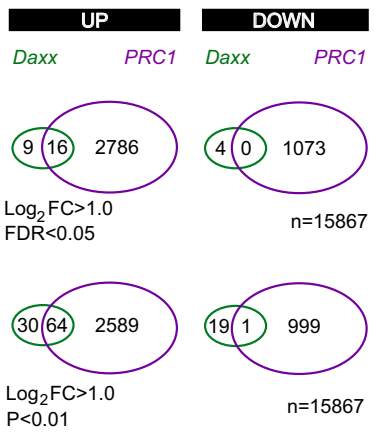

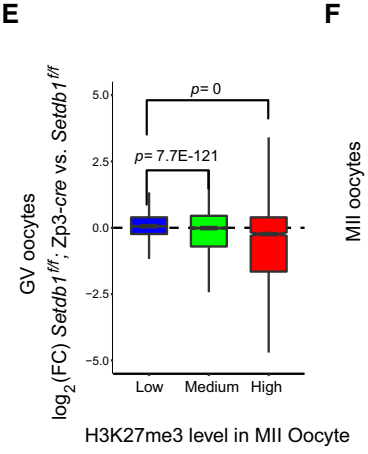

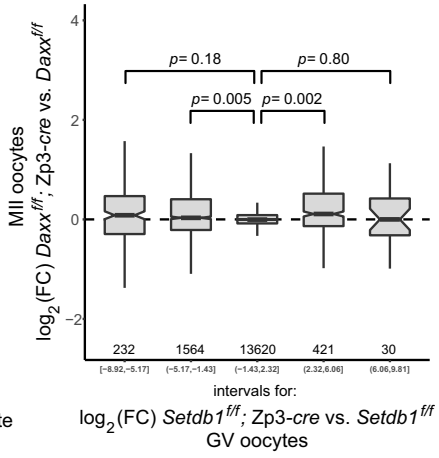

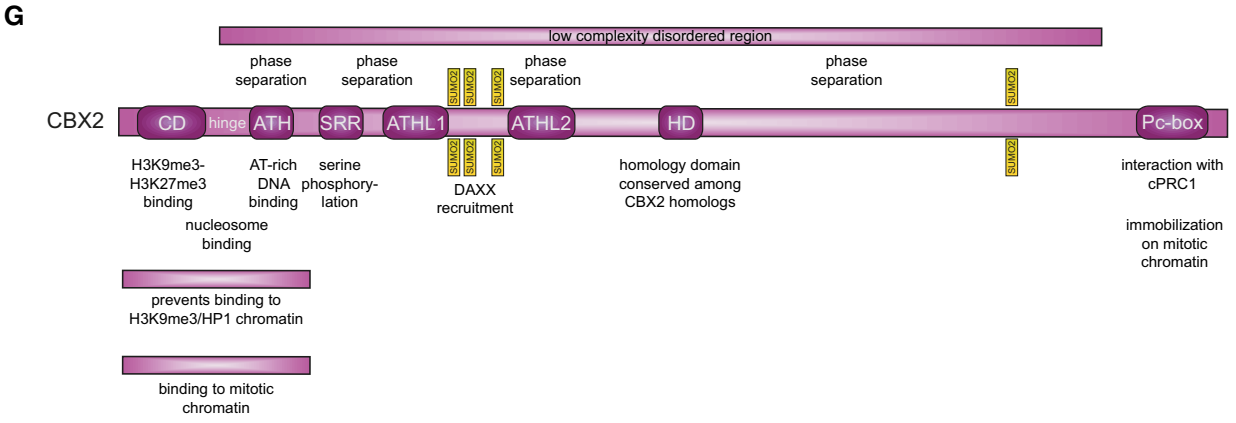

Figure EV5.